

Letter pubs.acs.org/macroletters

# Weakening of Solvation-Induced Ordering by Composition Fluctuation in Salt-Doped Block Polymers

Xian Kong,\* Kevin Jia-Yu Hou, and Jian Qin\*



Cite This: ACS Macro Lett. 2021, 10, 545-550



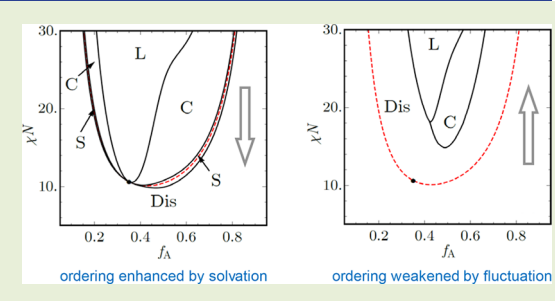
**ACCESS** I

Metrics & More

Article Recommendations

Supporting Information

ABSTRACT: The spontaneous ordering of block polymers doped with ions is affected by both selective solvation and long-range Coulombic interaction. The mean-field treatment was recently shown to overestimate the solvationinduced ordering, requiring a large solvation radius to fit experimental phase diagrams, which may be relieved by including composition fluctuations. Treating the composition fluctuations in such systems is challenging because of the need of resolving heterogeneous dielectric profile that couples with the ordering itself. Starting from a minimal model, we develop a Landau-Brazovskii expansion for the free energy of salt-doped block polymer near the ordering transition. It is found that the wavelength for typical composition



fluctuations first decreases with salt doping, due to Coulombic interaction, then increases due to ionic solvation. Two mechanisms that weaken the solvation-enhanced ordering are identified: the Brazovskii-type composition fluctuation that stabilizes disordered phase, and the coupling between mismatch in dispersion interaction and the dielectric permittivity through monomeric polarizability.

S alt-doped block polymer have been heavily investigated over the past decades, owing to its promise for safer energy storage and conversion. 1-3 Among various changes in morphological and transport behaviors, the susceptibility to a tiny amount of salt addition is particularly striking. 4-6 While this provides a facile tool to tune the assembled structure, it also calls for deeper theoretical understanding that is

Recent theoretical efforts<sup>5-7</sup> have transcribed the mean-field model of neat block polymers<sup>8-10</sup> to ion-doped systems. Selective ion-solvation and ionic correlation have been identified as important features of dielectrically heterogeneous copolymers. An unusual "chimney" channel for ordered phase has been predicted for fully compatible blocks,5 which is grossly consistent with existing experimental observations. 5,6,11 Recent attempts<sup>6</sup> further revealed a hidden, albeit narrow, entropic regime that competes with solvation effects and showed<sup>12</sup> that selective ion solvation alone captures morphological behaviors.

Our work is motivated by two considerations. First, ioninduced stabilization is expected to compete with the destabilizing composition fluctuation near the ordering transition. 13 Indeed, recent attempts to map phase diagrams from mean-field model with solvation treated at the Born level to experiments require solvation radii about an order of magnitude larger than physical ion size. <sup>12</sup> As solvation energy is inversely proportional to ion radius, <sup>7,14</sup> a large solvation radius essentially reduces the Born solvation effect. Several factors may compromise solvation effects, such as ion pair (or cluster) formation 4,15 and composition fluctuations beyond the mean-field level. We focus here on the more universal

fluctuation effects while leaving the ion-specific pairing or clustering correction to future studies.

Second, many current models treated the dispersion interaction described by the Flory-Huggins parameter and dielectric permittivity, two properties that both correlate to monomeric polarizabilities, independently, which is conceptually inconsistent. Motivated by recent work on polarizable field theory, 16 we shall reparameterize the dispersion interaction and the dielectric permittivity consistently using the monomeric polarizability, reassess the competition between solvation and composition fluctuation, and show that the "chimney" behavior is absent.

We use the "free" ion model developed recently for saltdoped polymers.<sup>6,12</sup> The mean-field critical points have been identified, and a mode-expansion in the weak-segregation regime is possible. The system contains  $n_C$  neutral AB diblock copolymer doped with monovalent salts. All polymer chains have N segments, among which Nf segments are of type A, and N(1-f) are of type B. The molar ratios between cations and type A segments are r. Measured in  $k_BT$ , the system Hamiltonian is  $\mathcal{H}=\mathcal{H}_{id}+\mathcal{H}_{FH}+\mathcal{H}_{B}+\mathcal{H}_{C}$ , where the ideal chain term  $\mathcal{H}_{id}$  and the Flory–Huggins term  $\mathcal{H}_{FH}$  are

Received: February 22, 2021 Accepted: April 16, 2021 Published: April 20, 2021





standard.<sup>6</sup> The additional terms are the Born solvation  $\mathcal{H}_B$  and the two-body Coulombic energy  $\mathcal{H}_C$ ,

$$\mathcal{H}_{B} = \frac{1}{\nu_{0}} \int d\mathbf{r} \frac{l_{0}}{2\epsilon_{r}(\mathbf{r})} \left( \frac{\hat{\phi}_{+}(\mathbf{r})}{\tilde{\nu}_{+}a_{+}} + \frac{\hat{\phi}_{-}(\mathbf{r})}{\tilde{\nu}_{-}a_{-}} \right)$$

$$\mathcal{H}_{C} = \frac{1}{2\nu_{0}^{2}} \int \int d\mathbf{r} d\mathbf{r}' \hat{\rho}_{q}(\mathbf{r}) g(\mathbf{r}, \mathbf{r}') \hat{\rho}_{q}(\mathbf{r}')$$
(1)

The microscopic volume fractions  $\hat{\phi}_{\alpha}$  ( $\alpha = A,B,+,-$ ) contain four components. Here  $l_0 \equiv e^2/(4\pi\epsilon_0 k_B T)$  is the Bjerrum length for vacuum, with e being the elementary charge and  $\epsilon_0$ the vacuum dielectric permittivity. The relative dielectric permittivity  $\epsilon_{\rm r}(r)$  is derived from polymer compositions. The relative volume in reference to a common factor  $v_0$ , and bead radii are denoted  $\tilde{\nu}_{\alpha}$  and  $a_{\alpha}$ , respectively. Without loss of generality, we assume  $\epsilon_{\rm A} > \epsilon_{\rm B}$  and  $a_+ < a_-$ . Although the physics is generic, we use parameters corresponding to PS-PEO doped with LiTFSI because of the relevance to experiments.<sup>6</sup> We use  $v_0 = 1 \text{ nm}^3$  and calculate the statistical segment length b from the packing length p = 0.4 nm as  $b = (v_0/p)^{1/2} = 1.58$ nm. This gives an invariant degree of polymerization  $\bar{N} \equiv Nb^6/\nu_0^2 = 622$  for the largest value N=40 we use, which overlaps with the range of  $\overline{N}$  values used in experiments.<sup>12</sup> The charge density fields are given by  $\hat{\rho} \equiv \hat{\phi}_{\perp}/\tilde{v}_{\perp} - \hat{\phi}/\tilde{v}_{\perp}$ . The kernel for coulombic interaction  $g(\mathbf{r}, \mathbf{r}')$  is obtained by inverting Poisson's equation with heterogeneous dielectric profile. More details of the Hamiltonian are available in the SI.

The role of electrostatics in microphase separation has been known in polyelectrolytes systems, 17-25 where electrostatic interaction drives microphase separation. In our system, however, electrostatic interaction only plays an auxiliary, modulating role for the self-assembly of block polymers.

The free energy is derived from the Hamiltonian by following the standard procedure. At the mean-field level, it only depends on the average density profiles  $\phi(\mathbf{r}) = [\phi_{A}(\mathbf{r}), \phi_{B}(\mathbf{r}), \phi_{+}(\mathbf{r}), \phi_{-}(\mathbf{r})]$ , and contains two terms,  $\mathcal{F}[\phi] = \mathcal{F}_{0}[\phi] + \mathcal{F}_{1}[\phi]$ . Here,  $\mathcal{F}_{0}[\phi]$  is from an ideal mixture with the same density profile as the interacting system, and  $\mathcal{F}_{1}[\phi]$  is the interaction term that is formally identical to the Hamiltonian.

An expansion of free energy in composition fluctuation is justified near the critical points shown in Figure 1.<sup>6</sup> For composition deviations from the mean-field values  $\bar{\phi}_{\alpha}$   $\delta\phi_{\alpha}(\mathbf{r}) \equiv \phi_{\alpha}(\mathbf{r}) - \bar{\phi}_{\alpha}$ , the free energy cost expanded to the quartic order reads

$$\begin{split} \Delta \mathcal{F} &= \frac{1}{2} \int \mathrm{d}\mathbf{q} \Gamma_{\mathbf{q}}^{(2)} \phi_{\mathbf{q}} \phi_{-\mathbf{q}} \\ &+ \frac{1}{3!} \int \int \mathrm{d}\mathbf{q}_{1} \mathrm{d}\mathbf{q}_{2} \Gamma_{\mathbf{q}_{1},\mathbf{q}_{2},\mathbf{q}_{3}}^{(3)} \phi_{\mathbf{q}_{1}} \phi_{\mathbf{q}_{2}} \phi_{\mathbf{q}_{3}} \\ &+ \frac{1}{4!} \int \int \int \mathrm{d}\mathbf{q}_{1} \mathrm{d}\mathbf{q}_{2} \mathrm{d}\mathbf{q}_{3} \Gamma_{\mathbf{q}_{1},\mathbf{q}_{2},\mathbf{q}_{3},\mathbf{q}_{4}}^{(4)} \phi_{\mathbf{q}_{2}} \phi_{\mathbf{q}_{3}} \phi_{\mathbf{q}_{4}} \end{split} \tag{2}$$

Here the expansion is around the homogeneous phase. The density fields are given in Fourier modes. By our convention, the Fourier integral includes a factor  $(2\pi)^{-3}$ , i.e.,  $\int d\mathbf{q} = \int \frac{d\mathbf{q}}{(2\pi)^3}$ , and the summation of wavenumbers in each term vanishes due to translational invariance. The coefficients

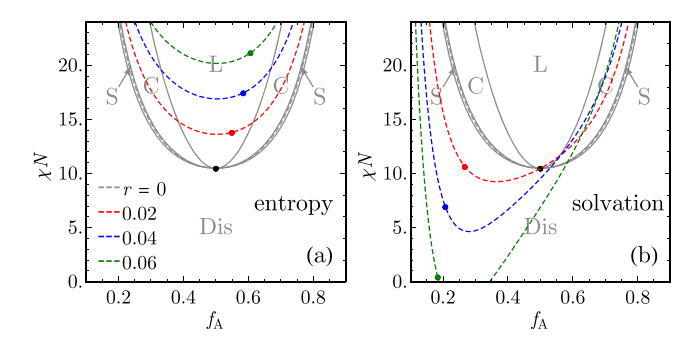


**Figure 1.** Mean-field phase diagram and spinodals from weak segregation theory (WST), for N=20 in (a) entropy regime with  $l_0=1$  nm, and (b) solvation regime with  $l_0=3$  nm. Solid lines: phase diagram of neat diblock. Dashed lines: spinodals from mean-field structure factor. Phase labels: L for lamellar, C for cylindrical, S for spherical.

 $\Gamma^{(2)}$ ,  $\Gamma^{(3)}$ , and  $\Gamma^{(4)}$  are vertex functions that include contributions from both the ideal free energy  $\mathcal{F}_0^{27}$  and the interaction term  $\mathcal{F}_{\rm I}$ . The Flory–Huggins interaction only contributes to  $\Gamma^{(2)}$ . The ion solvation and coulombic interaction contribute to all the higher-order terms. Explicit expressions of these coefficients are provided in the SI. Generally,  $\Gamma^{(3)}$  and  $\Gamma^{(4)}$  are dependent on the angles between wave vectors. However, it has been shown that the angle dependence of vertex functions only weakly modifies the phase behavior, at least at the Hartree level. <sup>28,29</sup> Therefore, we neglect the angle-dependence following the treatments of neat diblock polymers. <sup>13</sup>

The density waves  $\phi$  have four components: A-block, B-block, cation, and anion; the summation over these components are implicit in eq 2. In the incompressible melts of interest, the sum of density fluctuations vanish, i.e.,  $\sum_{\alpha}\delta\phi_{\alpha}(\mathbf{q})=0$ . The relevant composition fluctuation  $\delta\phi=(\delta\phi_{A},\delta\phi_{B},\delta\phi_{+},\delta\phi_{-})$  is orthogonal to the compression mode  $\varepsilon=(1,1,1,1)/2$  and can be expanded by any complete basis set that spans the subspace orthogonal to  $\varepsilon$ .<sup>6,30</sup> We choose the set of the solvation mode  $\mathbf{e}^{(1)}=(1,-1,1,-1)/2$ , antisolvation mode  $\mathbf{e}^{(2)}=(1,-1,-1,1)/2$ , and salting-out mode  $\mathbf{e}^{(3)}=(1,1,-1,-1)/2$ . The solvation mode drives smaller cations in-phase with more polar component A, while the antisolvation mode resists such trend. The salting-out mode drives salt out of polymers. An arbitrary composition fluctuation can be expanded as  $\delta\phi=\delta\psi_1\mathbf{e}^{(1)}+\delta\psi_2\mathbf{e}^{(2)}+\delta\psi_3\mathbf{e}^{(3)}$ .

Within the incompressible subspace, the vertex functions are reduced by contraction with  $\mathbf{e}_i$ . For instance, the contraction of  $\Gamma^{(2)}$  with  $\mathbf{e}^{(i)}$  gives a 3  $\times$  3 array,  $\hat{\gamma}_{\alpha\beta}^{(2)}(\mathbf{q}) = \Gamma_{ij}^{(2)}(\mathbf{q})\mathbf{e}_i^{(\alpha)}\mathbf{e}_j^{(\beta)}$ . Because the coefficients are evaluated in the disordered state,  $\hat{\gamma}^{(2)}$  only depends on the magnitude of wavevector,  $q = |\mathbf{q}|$ .

The spectra of  $\hat{\gamma}^{(2)}$  dictates the weight of composition fluctuations. Inside the disordered phase, all the eigenvalues of  $\hat{\gamma}^{(2)}$  are positive. At the spinodal, the smallest eigenvalue vanishes, with a corresponding eigenvector denoted by  $\mathbf{v}(q^*)$ , where  $q^*$  is the wavenumber of this critical mode. Close to the spinodal, the instability of the disordered phase is dominated by composition fluctuations proportional to  $\mathbf{V} = (\mathbf{e}^{(1)}, \mathbf{e}^{(2)}, \mathbf{e}^{(3)}) \cdot \mathbf{v}$ . For incompressible neat diblock copolymer,  $\mathbf{v} \propto (1, 1, 0)$ , giving rise to a composition mode  $\mathbf{V} \propto (1, -1, 0, 0)$ , as expected.

The behavior of critical mode v is similar in solvation (Figure 2a) and entropy regimes. The difference between

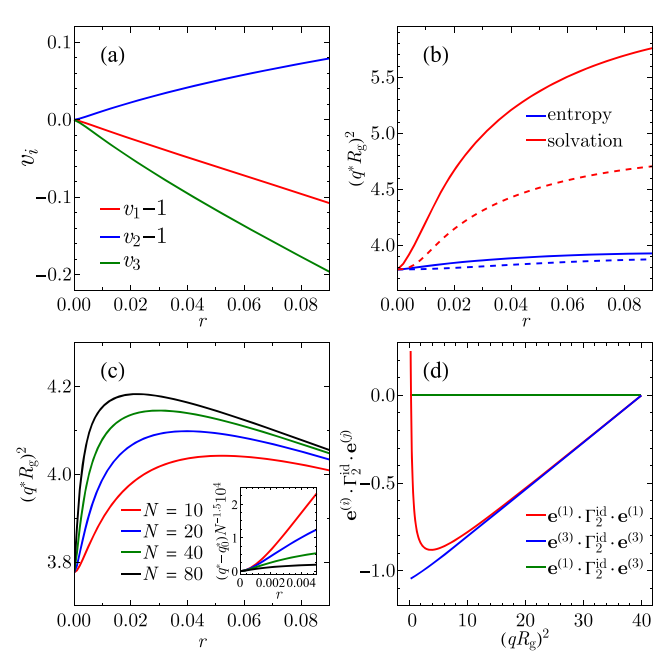


Figure 2. Variation of composition mode at the critical point for N=20: (a) mode vector  ${\bf v}$  in the solvation regime  $(l_0=3\text{ nm})$ ; (b) wavenumber  $q^*$  (solid) and  $q_0^*$  (dashed) in both entropy and solvation regimes. Variation of (c) peak wavenumber and (d) contributions to  $\gamma^{(2),\mathrm{id}}$  from different composition modes, at  $\chi N=10.495$ ,  $f_{\mathrm{A}}=0.5$ , and  $l_0=3$  nm. The inset in (c) rescales  $q^*-q_0^*$  with  $N^{-3/2}$ . (d) All curves are shifted with respect to the value at  $(qR_{\mathrm{g}})^2=40$ ; the other terms are not shown because  ${\bf e}^{(2)}\cdot\Gamma_2^{\mathrm{id}}\cdot{\bf e}^{(2)}={\bf e}^{(1)}\cdot\Gamma_2^{\mathrm{id}}\cdot{\bf e}^{(1)}\approx{\bf e}^{(1)}\cdot\Gamma_2^{\mathrm{id}}\cdot{\bf e}^{(2)}$  and  ${\bf e}^{(1)}\cdot\Gamma_2^{\mathrm{id}}\cdot{\bf e}^{(2)}\approx{\bf e}^{(2)}\cdot\Gamma_2^{\mathrm{id}}\cdot{\bf e}^{(3)}$ .

solvation and entropic regimes amounts to the degree of changes in  ${\bf v}$  upon doping, where  $v_i$  varies more slowly in entropic regime. The contribution from solvation mode decreases with elevated doping degree as the absolute value of  $v_1$  decreases. This is because, usually  $\tilde{v}_+ < \tilde{v}_-$ , upon equal molar doping of both ions, volume increases due to lithium ion addition is smaller. The contributions from both antisolvation  $(v_2)$  and salting-out  $(v_3)$  modes increase as the doping amount increases.

The second-, third-, and fourth-order vertex functions for composition fluctuations along mode  ${\bf v}$  are obtained by contraction, i.e.,  $\gamma^{(2)}=\hat{\gamma}^{(2)}_{ij}{\bf v}_i{\bf v}_j$ ,  $\gamma^{(3)}=\hat{\gamma}^{(3)}_{ijk}{\bf v}_i{\bf v}_j{\bf v}_k$ , and  $\gamma^{(4)}=\hat{\gamma}^{(4)}_{ijkl}{\bf v}_i{\bf v}_j{\bf v}_k{\bf v}_l$ . The critical point is identified by  $\gamma^{(2)}=\gamma^{(3)}=0.30$  In particular, the quadratic coefficient  $\gamma^{(2)}$  reads

$$\gamma^{(2)}(q) = \frac{F(qR_g)}{N} - 2\chi + (A_0 + A_s)r + \frac{A_c}{q^2}r^2$$
(3)

The first term is from polymer configurational and mixing entropy. The second term is Flory—Huggins interaction. The third term is derived from the translational entropy  $(A_0)$  and Born solvation free energy  $(A_s)$  of ions; they both scale linearly with r. The fourth term is from two-body Coulombic interaction (Supporting Information (SI)).

In the dilute limit, we expect the critical mode **v** to deviate from (1,1,0) by a correction proportional to *r* and have verified (SI,Figure S1) that  $\mathbf{v} \approx (1 + \eta_{12}r, 1 - \eta_{12}r, -\eta_3r)$ , with  $\eta_{12} = \frac{\eta_0}{2} \left( \frac{v_+}{a_+} - \frac{v_-}{a_-} \right)$  and  $\eta_3 = \eta_0 \left( \frac{v_+}{a_+} + \frac{v_-}{a_-} \right)$ , in which

$$\begin{split} \eta_0 &\equiv \frac{l_0(\epsilon_{\rm A} - \epsilon_{\rm B})}{4 v_{\rm A} \overline{\epsilon}^2}. \text{ The expressions to } A_0, \, A_{\rm s}, \, \text{and } A_{\rm c} \, \text{ are obtained} \\ \text{by contraction and given explicitly by } A_0 &= 2 v_{\rm A} \eta_0^2 \bigg(\frac{1}{a_+^2} + \frac{1}{a_-^2}\bigg), \\ A_{\rm s} &= 4 v_{\rm A} \eta_0^2 \bigg[\frac{2 \overline{\epsilon}}{l_0} \bigg(\frac{1}{a_+} + \frac{1}{a_-}\bigg) - \bigg(\frac{1}{a_+^2} + \frac{1}{a_-^2}\bigg)\bigg], \qquad \text{a n d} \\ A_{\rm c} &= \frac{4 \pi l_0 \eta_0^2}{\overline{\epsilon}} \bigg(\frac{1}{a_+} - \frac{1}{a_-}\bigg)^2. \, \text{ All these coefficients depend on } \eta_{0}^2, \\ \text{and vanish for } \epsilon_{\rm A} &= \epsilon_{\rm B}, \, \text{signifying the importance of selective solvation.} \end{split}$$

The ion translational entropy term  $A_0$  is always positive, stabilizing the disordered phase, which shifts the spinodal upward. Its dependence on  $l_0$  originates from the selective solvation, without which the ions are distributed uniformly. In this case, ions act as nonselective solvents, and higher-order wavevectors are needed to capture their localization at interfaces. The coefficient  $A_{\rm s}$  is positive for weak solvation but changes sign for strong solvation. In the latter case, its effect on spinodal is opposite to  $A_0$ , implying a competition between solvation and entropy, an effect first identified in polymer blends and recently verified in copolymers. The two-body Coulombic term is always positive because the local charge separation always induces a positive interaction energy.

Two terms in eq 3 vary with q. The configurational term  $F(qR_{\rm g})$  has a minimum at a nonzero wavenumber  $q_0^*$ , which depends on both composition and the mode vector  ${\bf v}$ . In the dilute limit  $(r \to 0)$ , the mode vector  ${\bf v} \to (1,1,0)$ , and  $q_0^*$  reduces to that given by Leibler. With tiny amount of salt addition, the coulombic term  $A_c r^2/q^2$  shifts the position of the minimum to a larger q at  $q^* > q_0^*$ , by a factor of order  $2A_c N^{3/2} r^2$ . The variation of peak positions at the critical points in both entropy and solvation regimes are shown in Figure 2b. The shift due to variation in critical composition is shown as dashed curve, and its departure from the solid curve highlights the contribution of Coulombic interaction.

A nonmonotonic variation of  $q^*$  with r is found at  $f_A = 0.5$ over a range of N values, as shown in Figure 2c. In the dilute limit,  $q^*$  increases with r and follows the scaling derived above,  $(q^*-q_0^*)\sim 2A_cN^{3/2}r^2$ ; the Figure 2c inset shows the collapse of data for  $(q^*-q_0^*)N^{-3/2}$  at small r. Previously, predicted increment in  $q^*$  was conjectured to result from ion solvation and neglect of ion volume; 15 here we see it originates from the Coulombic interaction, which in turn is triggered by charge separation due to ion solvation. More interesting is the decrease in  $q^*$  at higher salt doping, which can be rationalized by examining the contributions from different composition modes because the ideal term F is a weighted sum of these contributions. The contraction of the second vertex function with three independent composition modes are shown in Figure 2d. The contraction with the solvation mode  $e^{(1)}$  and the antisolvation mode  $e^{(2)}$  are equivalent to that for neat diblock polymers apart from an shift of order r and independent of q; these are related to ion translational entropy. In contrast, the contraction with  $e^{(3)}$  increases with q, which suggests that the decrease in  $q^*$  is favored by the salting-out mode.

The increase of  $q^*$  with r in the dilute regime has been found in previous theoretical studies. At higher doping level, while most experiments and simulation found  $q^*$  decreases with r, there are a few situations where  $q^*$  increases for changes nonmonotonically with r. It should be noted that our analysis about critical wavevector is

still based on mean-field treatment. The method we used here to include fluctuations does not consider its effect on shift in a critical wavevector. The trend found here may be masked by composition fluctuations, which we will investigate in the future.

Near the critical point, the transition is weakly discontinuous. The ordered phases are described by composition fluctuation that is proportional to mode vector V and that can be expanded using a superposition of plane waves  $\widetilde{\phi}(\mathbf{r}) = a_n \sum_{k=1}^n [\exp(i\mathbf{Q}_k \cdot \mathbf{r}) + \exp(-i\mathbf{Q}_k \cdot \mathbf{r})], \text{ where } \pm \mathbf{Q}_i, i = 1, ..., n \text{ are wavevectors with the magnitude } q^*, \text{ and with orientations specified by the symmetry of the phase.}^{27} \text{ We only}$ consider three classical phases (lamellar, hexagonal, and BCC) that can be described by the first harmonics. For other phases, such as lamellar-catenoid, contributions from higher harmonics must be included. 47,48 The free energy is obtained by substituting the density wave into eq 2, followed by minimization with respect to the amplitude of density wave  $a_n$ . The phase diagram generated by this analysis compares quantitatively to the iPSCF calculations,6 as demonstrated in SI, Figure S2. For regions far from the critical point, the discontinuity in phase transition becomes more severe, and the contributions from higher harmonics are important. 28,29,48 For this reason, we do not expect our theory to be accurate far from the critical point, although the agreement between our analytical calculation and numerical iPSCF is still satisfactory.

To examine the fluctuation effects, we map the free energy onto the Brazovskii form by expanding  $\gamma^{(2)}$  around  $q^*$  as  $\gamma^{(2)}(q) = 2\mathbf{v}_{\rm A}\mathbf{v}_{\rm B}(\chi-\chi_{\rm s}) + c^2(q-q^*)^2$ , where  $c^2 = 1/2$   $\partial^2\gamma^{(2)}(q^*)/\partial q^2$  is related to the curvature of  $\gamma^{(2)}$  at  $q^*$ , and  $\chi_{\rm s}$  is the spinodal  $\chi$ -value. The fluctuation-corrected phase diagrams obtained by an approach similar to ref 13 are compared to the mean-field predictions in Figure 3 for N=20

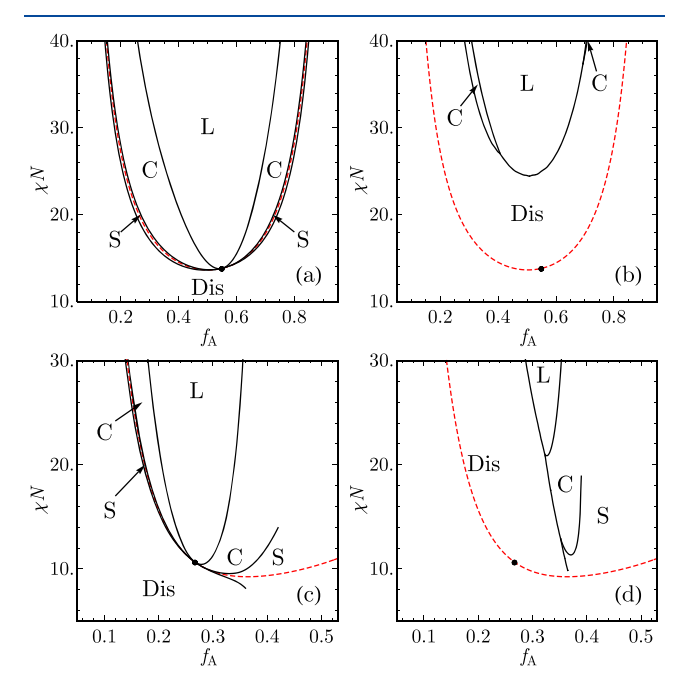


**Figure 3.** Mean-field (a) and fluctuation-corrected (b) phase diagrams in the entropy regime with  $l_0 = 1$  nm. Corresponding phase diagrams (c,d) in the solvation regime with  $l_0 = 3$  nm. Red dashed line: spinodal from mean-field structure factor. All panels: N = 20, r = 0.02. See SI for results at N = 10 and N = 40.

and in SI, Figures S3 and S4, for N=10 and 40, respectively. In both entropy and solvation regimes, the fluctuation correction destabilizes the ordered phase and shifts the phase diagram upward. In the entropy regime, the extra shift is several times stronger than the effect due to entropy alone. In the experimentally more relevant solvation regime, the effect competes with solvation. In particular, the upper-shift in the ordering transition into the lamellar phase is quite pronounced. The other known effects in the Fredrickson—Helfand theory, <sup>13</sup> such as the direct ordering transition into the hexagonal phase, are maintained.

The above theory treated  $\chi$  and  $\epsilon_{\rm r}$  independently which, although commonly adopted, is conceptually inconsistent. The dielectric permittivity can be approximately related to the monomeric polarizability through the Clausius–Mossotti relation by  $\frac{\epsilon_{\rm r}-1}{\epsilon_{\rm r}+2}=\alpha$ . The average dielectric permittivity of monomeric mixtures can be estimated using the Maxwell–Garnett mixing rule,  $\frac{\epsilon_{\rm r}-1}{\epsilon_{\rm r}+2}=\frac{1}{\nu}\sum_i\phi_i\alpha_i$ , where  $1/\nu$  is the average density. Meanwhile, it is known that the Flory–Huggins parameter can be related to monomeric polarizability through the cohesive energy density,  $^{16}\chi=c_\chi(\alpha_{\rm A}-\alpha_{\rm B})^2$ , where  $c_\chi$  is a parameter that is related to the volume and charge distribution of the monomers.

The new and consistent parametrization with polarizabilities brings remarkable changes in the phase behavior. Figure 4a

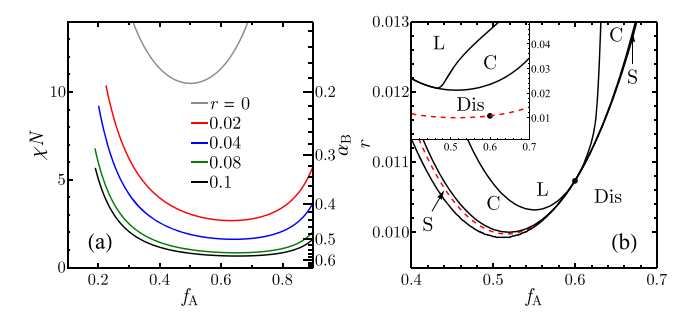


**Figure 4.** Spinodal and phase diagrams from polarizability-based parametrization. (a) Spinodals against  $f_{\rm A}$  and  $\alpha_{\rm B}$  for different r, at N=20,  $\alpha_{\rm A}=0.70$ ,  $c_{\chi}=2.0$ ,  $l_0=3$  nm. (b) Mean-field phase diagram at N=20,  $\alpha_{\rm A}=0.70$ ,  $\alpha_{\rm B}=0.32$ ,  $c_{\chi}=0.5$ , and  $l_0=3$  nm, and fluctuation-corrected phase diagram (inset); red dashed line, spinodal from mean-field structure factor

shows that, as r increases, the spinodal line in the  $\chi$ -f plane shifts downward. Unlike the case in previous parametrization, we found no chimney behavior. Instead, the spinodal converges to a limiting one above  $\chi=0$  as r increases. This is because, as the incompatibility between two polymer blocks diminishes ( $\chi\to0$ ),  $\alpha_{\rm A}$  and  $\alpha_{\rm B}$  becomes similar and the dielectric constant between two blocks diminishes.

By fixing  $\alpha_A$  and  $\alpha_B$  from polymer permittivity, we generate both mean-field and fluctuation-corrected phase diagrams, shown in Figure 4b. It is found that the wide lamellar window is replaced by the hexagonal phase when the fluctuation correction is turned on, and the amount of salt needed to induce ordering is nearly doubled.

In summary, we showed the weakening of solvationenhanced ordering due to the composition fluctuation and the coupling between dispersion interaction and dielectric screening. Several relevant physics have been neglected. For instance, ion pairing or clustering and liquid-state correlation

may be particularly relevant at high doping-level; the fluctuation correction to the scattering function itself may lead to further reduction in  $q^*$  as was evident in the neutral diblock polymers. <sup>29,45,46</sup> Nevertheless, our work is a minimum treatment of composition fluctuation in ion-doped polymers, which provides the basis for future generalization and comparison to polarizable field theoretical calculations. <sup>16,49,50</sup>

### ASSOCIATED CONTENT

# Supporting Information

The Supporting Information is available free of charge at https://pubs.acs.org/doi/10.1021/acsmacrolett.1c00107.

Expression of interaction contribution to free energy, and expansion coefficients; a scaling analysis of the shift in the peak position of structure factor; validation of analytical expressions for the critical eigenvector; comparison of phase diagrams from WST and iPSCF; phase diagrams for N=10 and 40 (PDF)

#### AUTHOR INFORMATION

#### **Corresponding Authors**

Jian Qin — Department of Chemical Engineering, Stanford University, Stanford, California 94305, United States;

o orcid.org/0000-0001-6271-068X; Email: jianq@

orcid.org/0000-0001-6271-068X; Email: jianq@stanford.edu

Xian Kong — Department of Chemical Engineering, Stanford University, Stanford, California 94305, United States; orcid.org/0000-0001-5602-6347; Email: xiankong@stanford.edu

# Author

Kevin Jia-Yu Hou — Department of Chemical Engineering, Stanford University, Stanford, California 94305, United States

Complete contact information is available at: https://pubs.acs.org/10.1021/acsmacrolett.1c00107

### Notes

The authors declare no competing financial interest.

## ACKNOWLEDGMENTS

This research has been supported by the National Science Foundation CAREER Award through DMR-1846547 and the Assistant Secretary for Energy Efficiency and Renewable Energy, Office of Vehicle Technologies of the U.S. Department of Energy through the Advanced Battery Materials Research (BMR) Program (Battery500 Consortium).

#### REFERENCES

- (1) Mao, G.; Saboungi, M.-L.; Price, D. L.; Armand, M. B.; Howells, W. S. Structure of Liquid PEO-LiTFSI Electrolyte. *Phys. Rev. Lett.* **2000**, *84*, 5536–5539.
- (2) Hallinan, D. T.; Balsara, N. P. Polymer electrolytes. Annu. Rev. Mater. Res. 2013, 43, 503-525.
- (3) Miller, T. F., III; Wang, Z.-G.; Coates, G. W.; Balsara, N. P. Designing polymer electrolytes for safe and high capacity rechargeable lithium batteries. *Acc. Chem. Res.* **2017**, *50*, 590–593.
- (4) Nakamura, I.; Balsara, N. P.; Wang, Z.-G. Thermodynamics of ion-containing polymer blends and block copolymers. *Phys. Rev. Lett.* **2011**, *107*, 1–5.
- (5) Sing, C.; Zwanikken, J. W.; Olvera de la Cruz, M. Electrostatic control of block copolymer morphology. *Nat. Mater.* **2014**, *13*, 694–698.

- (6) Hou, K. J.; Qin, J. Solvation and entropic regimes in ion-containing block copolymers. *Macromolecules* **2018**, *51*, 7463.
- (7) Wang, Z.-G. Effects of ion solvation on the miscibility of binary polymer blends. *J. Phys. Chem. B* **2008**, *112*, 16205–16213.
- (8) Bates, F. S.; Fredrickson, G. H. Block copolymer thermodynamics: theory and experiment. *Annu. Rev. Phys. Chem.* **1990**, *41*, 525–557.
- (9) Matsen, M. W.; Schick, M. Stable and unstable phases of a diblock copolymer melt. *Phys. Rev. Lett.* **1994**, 72, 2660–2663.
- (10) Matsen, M. W.; Bates, F. S. Unifying weak- and strong-segregation block copolymer theories. *Macromolecules* **1996**, *29*, 1091–1098.
- (11) Loo, W. S.; Jiang, X.; Maslyn, J. A.; Oh, H. J.; Zhu, C.; Downing, K. H.; Balsara, N. P. Reentrant phase behavior and coexistence in asymmetric block copolymer electrolytes. *Soft Matter* **2018**, *14*, 2789–2795.
- (12) Hou, K. J.; Loo, W.; Balsara, N.; Qin, J. Comparing experimental phase behavior of ion-doped block copolymers with theoretical predictions based on selective ion solvation. *Macromolecules* **2020**, *53*, 3956.
- (13) Fredrickson, G. H.; Helfand, E. Fluctuation effects in the theory of microphase separation in block copolymers. *J. Chem. Phys.* **1987**, 87, 697.
- (14) Wang, Z.-G. Fluctuation in electrolyte solutions: the self energy. *Phys. Rev. E* **2010**, *81*, 021501.
- (15) Nakamura, I.; Wang, Z.-G. Salt-doped block copolymers: ion distribution, domain spacing and effective  $\chi$  parameter. *Soft Matter* **2012**, *8*, 9356.
- (16) Martin, J. M.; Li, W.; Delaney, K. T.; Fredrickson, G. H. Statistical field theory description of inhomogeneous polarizable soft matter. *J. Chem. Phys.* **2016**, *145*, 154104.
- (17) Borue, V. Y.; Erukhimovich, I. Y. A statistical theory of weakly charged polyelectrolytes: fluctuations, equation of state and microphase separation. *Macromolecules* **1988**, *21*, 3240–3249.
- (18) Joanny, J.; Leibler, L. Weakly charged polyelectrolytes in a poor solvent. *J. Phys. (Paris)* **1990**, *51*, 545–557.
- (19) Khokhlov, A.; Nyrkova, I. Compatibility enhancement and microdomain structuring in weakly charged polyelectrolyte mixtures. *Macromolecules* **1992**, *25*, 1493–1502.
- (20) Dormidontova, E. E.; Erukhimovich, I. Y.; Khokhlov, A. R. Microphase separation in poor-solvent polyelectrolyte solutions: Phase diagram. *Macromol. Theory Simul.* **1994**, *3*, 661–675.
- (21) Gritsevich, A. Phase diagrams of polyelectrolyte solutions in poor solvents and of polyelectrolyte globules with allowance for microphase separation and fluctuation effects. *Polym. Sci., Ser. A* **2008**, 50, 58–67.
- (22) Shi, A.-C.; Noolandi, J. Theory of inhomogeneous weakly charged polyelectrolytes. *Macromol. Theory Simul.* **1999**, *8*, 214–229.
- (23) Dobrynin, A.; Erukhimovich, I. Y. Weak crystallization and structural phase transitions in weakly charged polyelectrolyte systems. *Zh. Eksp. Teor. Fiz* **1991**, *99*, 1344–1359.
- (24) Nyrkova, I.; Khokhlov, A.; Kramarenko, Y. Y. Possibility of microphase separation in polyelectrolyte systems. *Polym. Sci. U.S.S.R.* **1990**, 32, 852–861.
- (25) Rumyantsev, A. M.; de Pablo, J. J. Microphase Separation in Polyelectrolyte Blends: Weak Segregation Theory and Relation to Nuclear "Pasta. *Macromolecules* **2020**, *53*, 1281–1292.
- (26) Fredrickson, G. The Equilibrium Theory of Inhomogeneous Polymers; Oxford University Press, 2013.
- (27) Leibler, L. Theory of microphase separation in block copolymers. *Macromolecules* **1980**, *13*, 1602–1617.
- (28) Mayes, A.; de la Cruz, M. O. Concentration fluctuation effects on disorder—order transitions in block copolymer melts. *J. Chem. Phys.* **1991**, *95*, 4670–4677.
- (29) Olvera de la Cruz, M. Transitions to periodic structures in block copolymer melts. *Phys. Rev. Lett.* **1991**, *67*, 85.
- (30) Qin, J.; Bates, F. S.; Morse, D. C. Phase behavior of nonfrustrated ABC triblock copolymers: weak and intermediate segregation. *Macromolecules* **2010**, *43*, 5128–5136.

- (31) Fredrickson, G. H.; Leibler, L. Theory of block copolymer solutions: nonselective good solvents. *Macromolecules* **1989**, 22, 1238–1250.
- (32) Brown, J. R.; Seo, Y.; Hall, L. M. Ion correlation effects in salt-doped block copolymers. *Phys. Rev. Lett.* **2018**, *120*, 127801.
- (33) Young, W.-S.; Epps, T. H. Salt doping in PEO-containing block copolymers: counterion and concentration effects. *Macromolecules* **2009**, *42*, 2672–2678.
- (34) Teran, A. A.; Balsara, N. P. Thermodynamics of block copolymers with and without salt. *J. Phys. Chem. B* **2014**, *118*, 4–17.
- (35) Panday, A.; Mullin, S.; Gomez, E. D.; Wanakule, N.; Chen, V. L.; Hexemer, A.; Pople, J.; Balsara, N. P. Effect of Molecular Weight and Salt Concentration on Conductivity of Block Copolymer Electrolytes. *Macromolecules* **2009**, 42, 4632–4637.
- (36) Loo, W. S.; Jiang, X.; Maslyn, J. A.; Oh, H. J.; Zhu, C.; Downing, K. H.; Balsara, N. P. Reentrant phase behavior and coexistence in asymmetric block copolymer electrolytes. *Soft Matter* **2018**, *14*, 2789–2795.
- (37) Chintapalli, M.; Timachova, K.; Olson, K. R.; Mecham, S. J.; DeSimone, J. M.; Balsara, N. P. Lithium Salt Distribution and Thermodynamics in Electrolytes Based on Short Perfluoropolyether-block-Poly (ethylene oxide) Copolymers. *Macromolecules* **2020**, 53, 1142–1153.
- (38) Loo, W. S.; Balsara, N. P. Organizing thermodynamic data obtained from multicomponent polymer electrolytes: Salt-containing polymer blends and block copolymers. *J. Polym. Sci., Part B: Polym. Phys.* **2019**, *57*, 1177–1187.
- (39) Loo, W. S.; Galluzzo, M. D.; Li, X.; Maslyn, J. A.; Oh, H. J.; Mongcopa, K. I.; Zhu, C.; Wang, A. A.; Wang, X.; Garetz, B. A.; et al. Phase behavior of mixtures of block copolymers and a lithium salt. *J. Phys. Chem. B* **2018**, *122*, 8065–8074.
- (40) Sethuraman, V.; Mogurampelly, S.; Ganesan, V. Multiscale simulations of lamellar PS-PEO Block copolymers doped with LiPF<sub>6</sub> ions. *Macromolecules* **2017**, *50*, 4542–4554.
- (41) Ruzette, A.-V. G.; Soo, P. P.; Sadoway, D. R.; Mayes, A. M. Melt-formable block copolymer electrolytes for lithium rechargeable batteries. *J. Electrochem. Soc.* **2001**, *148*, A537.
- (42) Huang, J.; Tong, Z.-Z.; Zhou, B.; Xu, J.-T.; Fan, Z.-Q. Salt-induced microphase separation in poly ( $\varepsilon$ -caprolactone)-b-poly (ethylene oxide) block copolymer. *Polymer* **2013**, *54*, 3098–3106.
- (43) Naidu, S.; Ahn, H.; Gong, J.; Kim, B.; Ryu, D. Y. Phase behavior and ionic conductivity of lithium perchlorate-doped polystyrene-b-poly (2-vinylpyridine) copolymer. *Macromolecules* **2011**, *44*, 6085–6093.
- (44) Sethi, G. K.; Jung, H. Y.; Loo, W. S.; Sawhney, S.; Park, M. J.; Balsara, N. P.; Villaluenga, I. Structure and thermodynamics of hybrid organic—inorganic diblock copolymers with salt. *Macromolecules* **2019**, *52*, 3165–3175.
- (45) Qin, J.; Morse, D. C. Fluctuations in symmetric diblock copolymers: testing theories old and new. *Phys. Rev. Lett.* **2012**, *108*, 238301.
- (46) Barrat, J.-L.; Fredrickson, G. H. Collective and single-chain correlations near the block copolymer order—disorder transition. *J. Chem. Phys.* **1991**, *95*, 1281–1289.
- (47) Olvera de La Cruz, M.; Mayes, A.; Swift, B. Transition to lamellar-catenoid structure in block-copolymer melts. *Macromolecules* **1992**, 25, 944–948.
- (48) Jones, J.; Olvera de la Cruz, M. Transitions to periodic structures: Higher harmonic corrections with concentration fluctuations. *J. Chem. Phys.* **1994**, *100*, 5272–5279.
- (49) Nakamura, I.; Shi, A.-C.; Wang, Z.-G. Ion solvation in liquid mixtures: effects of solvent reorganization. *Phys. Rev. Lett.* **2012**, *109*, 257802.
- (50) Nakamura, I. Ion Solvation in Polymer Blends and Block Copolymer Melts: Effects of Chain Length and Connectivity on the Reorganization of Dipoles. *J. Phys. Chem. B* **2014**, *118*, 5787–5796. PMID: 24806716